Hindawi
Journal of Chemistry
Volume 2019, Article ID 8359491, 9 pages
https://doi.org/10.1155/2019/8359491

Research Article

Adsorptive Removal of Dyes from Aqueous Solution by $KMnO_4$-Modified Rice Husk and Rice Straw

Xiaodong Li and Yunjin Li

Department of Basic Science, Jilin Jianzhu University, Changchun 130118, China

Correspondence should be addressed to Xiaodong Li; lxdjlju@163.com

Received 3 January 2019; Revised 15 June 2019; Accepted 4 July 2019; Published 1 August 2019

Academic Editor: Mohammad A. Al-Ghouti

Rice husk (RH) and rice stalk (RS), the abundant biomasses, have been tentatively explored as the renewable biochar which were prepared by means of hydrothermal and activation processes, and the synthetic procedure is quite simple and easy to be scaled up for industrial applications. In this work, the removal of malachite green (MG) was investigated by $KMnO_4$-treated RH and RS as the efficient adsorbents at various experimental conditions. Various operational parameters such as initial dye concentration, adsorbent dosage, and solution temperature in batch systems were investigated on the use of RH and RS. The adsorption isotherm model (Langmuir and Freundlich isotherms), kinetic model (pseudo-first-order, pseudo-second-order, and Elovich models), and the adsorption mechanism (intraparticle diffusion and Boyd models) were studied. It showed that that the Langmuir model and Elovich model are suitable for describing the adsorption process, and the diffusion rate of surface adsorption and the particle diffusion rate jointly affect the reaction rate of adsorption. This facile, efficient, and template-free synthesis strategy holds great promise for preparing novel porous biochar from renewable biomass resources for application in adsorbents.

1. Introduction

The disposal of textile wastewater is currently a major problem from a global viewpoint [1]. Textile industries produce a lot of wastewater, which contains several contaminants, including acidic or caustic dissolved solids, toxic compounds, and dyes [2]. Among textile effluents, synthetic dyes are a necessity in various significant industries such as the leather, paper, and textile industries for its colour-giving properties. For example, the wastewaters produced by dye manufacturing and textile finishing industries contain heavy metals, which are used as a mordant in the dyeing process [3]. The discharge of untreated effluent-containing dyes into aquatic ecosystems has been an outcome of the rapid increase in population coupled with high industrial-scale operations. Nowadays, the dyes in water can be removed by various physical and chemical treatment methods such as biodegradation, ion exchange, chemical precipitation, reverse osmosis, coagulation flocculation, etc. However, the different physical and chemical properties of dye make the treatment of dye wastewaters more challenging. Adsorption, which is the most economical and effective, has become the most preferred method for the dye removal [4, 5]. Therefore, the development of new adsorbents with high efficiency, economy, and easy solid-liquid separation has become the focus of research.

The commonly used adsorbents include activated carbon adsorbents and metal and nonmetal oxide adsorbents. The most representative adsorbent is activated carbon, and the adsorption performance of activated carbon is quite good. However, disadvantages of the activated carbon include relatively expensive and the lower mechanical strength. Therefore, there is a great interest in finding inexpensive and effective alternatives to the existing commercial activated carbon, such as molecular sieve, silica gel, active aluminum, polymer adsorbent and biological adsorbent, and so on. Our previous work has shown that the mesoporous molecular sieve (MCM-41, SBA-15) has a good adsorption effect on

metals or dyes. However, the preparation method of the mesoporous molecular sieve is complex, and it demands high energy of prepared adsorbent. Furthermore, this technology has some drawbacks such as consuming a lot of template and water [6, 7]. Biomass adsorbents have a good adsorption effect due to the natural lignocellulosic matrix, e.g., wheat straw, peanut shell, moss peat, bagasse fly ash, tree fern, gram husk, and saw dust for dye removal [8–11].

Rice husk (RH) and rice straw (RS) are the main agricultural biomass in China. Their main components include cellulose (about 35 wt.%, 37.4 wt.%), hemicellulose (about 25 wt.%, 44.9 wt.%), lignin (about 20 wt.%, 4.9 wt.%), and silica fume (about 20 wt.%, 13.1 wt.%) [12, 13]. Nevertheless, RH and RS were discarded and rotted away into soil without effective utilizations. The novel biochar prepared by RH and RS, in which organic moieties are distributed in the framework, forms a covalently bonded network. The biochar has attracted more and more attention due to its good catalytic performance, tunable structure, and low cost of raw materials.

The process for production of biochar is one of the feasible methods. Biochar is being developed as a candidate with great potential for climate change mitigation. Hydrothermal carbonization (HTC) refers to the technology of heating biomass in aqueous suspension to 180–250°C in a closed system to produce energy-intensive, high-carbon, and hydrophobic solid hydrates [14–16]. Hydrolysis, dehydration, decarboxylation, aromatization, and condensation polymerization occur at high water content [17]. Thus, hydrates are usually composed of aliphatic compounds rather than aromatic compounds like biochar [18].

Biochar can be generally acquired by simple carbonization and activation treatment of cheap and easily available natural biomass wastes or carbonaceous minerals that are activated by different porogens. Herein, RH and RS were employed as precursor for preparation of biochar by hydrothermal carbonization and $KMnO_4$ oxidation. The remarkably enhanced specific surface areas, versatile pore texture with the coexistence of both micropores, and meso/macropores, apparently increased hydrophilicity which made the as-prepared biochar high-performance adsorbing materials. The adsorption mechanism of MG was investigated.

2. Experimental

2.1. Materials. Rice husks and rice stalks were taken from the farmland around Changchun, washed, and ultrasonically removed from the surface adherends, and then dried at 60°C in an oven to constant weight; MG, formulated into a stock solution with a mass concentration of 1 g·L^{-1}, was diluted to the required concentration according to the experimental needs; $KMnO_4$, NaCl, NaOH, and HCl are all analytically pure; experimental water is deionized water.

2.2. Preparation of $KMnO_4$-Modified Hydrothermal Biochar. Two grams of rice husk was put into a polytetrafluoroethylene lining containing 20 mL of deionized water or $KMnO_4$ solution (0.1 mol·L^{-1}, 0.5 mol·L^{-1}, and 1 mol·L^{-1}), fully infiltrated and placed in the reaction vessel, and then heated to 180°C for 4 h. After cooling down to room temperature, the resulting product was cross-washed with acetone and deionized water until the filtrate was nearly colorless. Samples were collected by vacuum filtration, washed with deionized water until pH of the washed water was around 7.0, and dried at room temperature for 24 h. The hydrothermal biochar prepared from the rice husk was recorded as RH, $KRH_{0.1}$, $KRH_{0.5}$, and KRH_1. The rice straw was used as raw material to prepare samples RS, $KRS_{0.1}$, $KRS_{0.5}$, and KRS_1 using the same procedure.

2.3. Characterization and Analysis. The morphologies of KRH_x and KRS_x were characterized by using scanning electron microscope (SEM) (JSM-5600LV, JEOL, Japan). Surface functional group characteristics before and after biochar adsorption were determined by the FTIR Spectrum-100 Fourier-transform infrared spectrometer using conventional KBr pellets in the 4000–400 cm^{-1} range. The zero point of charge (pH_{pzc}) of the sample is determined by salt addition method [19]: a certain amount of $NaNO_3$ (0.01 M) solution was taken in different titration flasks. NaOH (0.1 M) and HNO_3 (0.1 M) solutions were added to adjust the initial pH of the suspension to 2–12 (pH_i). Then, 0.2 g sample was added to each flask and was shaken for 4 h on an ultrasonic cleaner. Final pH of the solution was recorded. The pH_{pzc} values were determined by plotting a function of pH_f-pH_i.

2.4. Batch Adsorption Experiment. The effects of initial dye concentration, adsorbent dosage, and solution temperature for adsorption of MG onto KRH_x and KRS_x were studied.

The concentration of MG in the solution was determined using an ultraviolet-visible spectrophotometer (UV-1700), and the adsorption amount q_t and removal rate η of the sample were calculated by using the following formulas:

$$q_t = \frac{(C_0 - C_t)V}{m}, \quad (1)$$

$$\eta = \frac{1 - C_t}{C_0}, \quad (2)$$

where C_0 and C_t (mg·L^{-1}) are the initial and final equilibrium concentrations of MG in solution, respectively, V (mL) is the volume of solution, and m (mg) is the mass of the adsorbent.

3. Results and Discussion

3.1. Characterization Analysis. As shown in Figure 1, $KRS_{0.5}$ and $KRH_{0.5}$ were regular rod-shaped and cubic-shaped particles in size of several micrometers, and the surface of particles was rather rough. Meanwhile, the SEM images of $KRS_{0.5}$ and $KRH_{0.5}$ reveal the presence of abundant

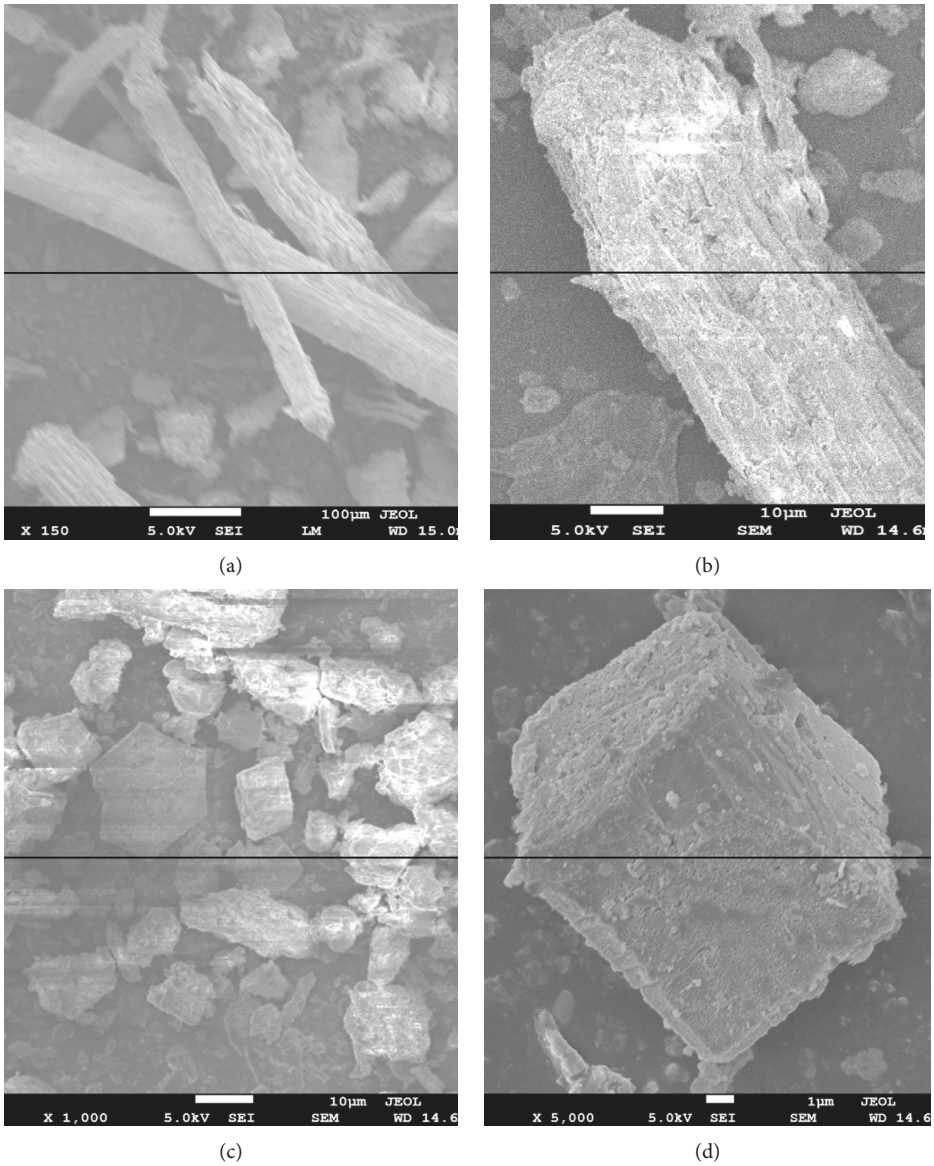

(a) (b) (c) (d)

Figure 1: SEM of $KRH_{0.5}$ and $KRS_{0.5}$.

mesopores and micropores with several nanometers in size, which was beneficial to improve adsorption performance and recycling. A large number of white crystals were attached to the surface, probably because after the treatment of $KMnO_4$, more oxygen-containing functional groups were generated on the surface of hydrothermal biochar, generating MnO_2 and loading on the surface (Table 1).

The FT-IR spectrum of the four groups of samples displayed a number of absorption peaks (Figure 2(a)), which indicated the presence of different types of functional groups in the biosorbent. The O-H stretching vibration of hydroxyl and carboxyl groups on the surface of KRH_x or KRS_x was confirmed by a broad band between 3410 and 3440 cm^{-1}. At 2910–2920 cm^{-1}, it was the stretching vibration peak of aliphatic compound C-H [20], and the peak intensity of KRH_x was larger than that of KRS_x. The characteristic peak of C=C bond exists at 1630 cm^{-1}, indicating that aromatization of sugar occurred during hydrothermal carbonization [21]. The bands at 1280–1430 cm^{-1} are attributed to absorption by C-O, O-H, $-CH_3$, or $-CH_2$ stretching vibration, which indicates the presence of reactive oxygen-containing functional groups on the surface of the sample [22]. The

Table 1: Parameters of pore structure of the samples.

Sample	BET surface area ($m^2 \cdot g^{-1}$)	Pore volume ($cm^3 \cdot g^{-1}$)	Average pore diameter (nm)
RH	15.77	0.05	3.83
$KRH_{0.1}$	6.77	0.04	3.81
$KRH_{0.5}$	20.61	0.27	3.42
RS	7.54	0.11	4.32
KRS_1	27.02	0.08	3.83

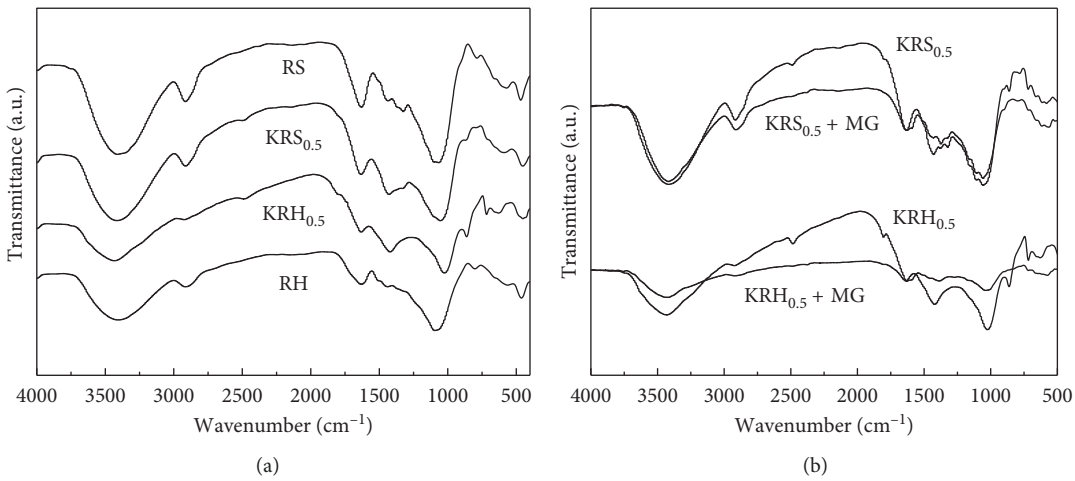

Figure 2: (a) The FT-IR spectra of RH, $KRH_{0.5}$, RS, and $KRS_{0.5}$. (b) The FT-IR spectra of $KRH_{0.5}$ and $KRS_{0.5}$ before and after MG adsorption.

strong band at 1050 cm^{-1} was assigned to C-O stretching in cellulose, hemicelluloses, and lignin or C-O-C stretching in cellulose and hemicelluloses. The small sharp band at 802–862 cm^{-1} was originated from the β-glucosidic linkage between the sugar units in hemicelluloses and cellulose [23]. Finally, the presence of a band around 471 cm^{-1} was generally attributable to the bending vibration of O-Si-O [24].

By comparing the spectra of $KRH_{0.5}$ and $KRS_{0.5}$ after MG adsorption (Figure 2(b)), it can be found out that the slight wider peaks between 1630 and 1050 cm^{-1} indicate that the original π-conjugated aromatic structure and dye form a stable structure with less energy.

3.2. Effect of Dosage on the Adsorption of MG. As shown in Figure 3, with the increase of dosage, removal rate of dye increased, but adsorption amount of MG decreased. This may be attributed to that most of the adsorption sites of $KRH_{0.5}$ and $KRS_{0.5}$ were still unsaturated and the amount of adsorption per unit mass is low. Therefore, in order to make full use of adsorbent's adsorption point position and exert its maximum adsorption capacity, in this paper, 0.05 g of biochar is taken as the optimal dosage of adsorbent.

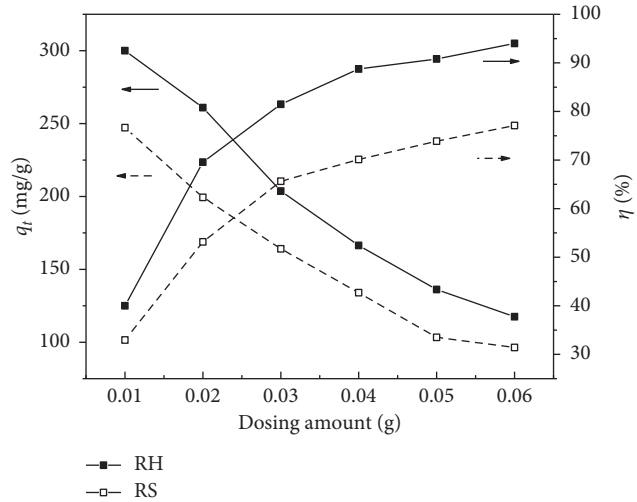

Figure 3: Effect of $KRH_{0.5}$ and $KRS_{0.5}$ dosage on the adsorption of MG.

3.3. Effect of Initial Concentration and Adsorption Isotherm

3.3.1. Effect of Initial Concentration of MG. The initial dye concentration has a pronounced effect on its removal from aqueous solutions. The adsorption of MG on $KRH_{0.5}$ and $KRS_{0.5}$ was investigated as a function of contact time at the different initial MG concentrations in the range of 0–180 min at room temperature, and the results are presented in Table 2. It was found that the removal of dye by $KRH_{0.5}$ increased from 74.64% to 92.28% with decreasing initial concentration of MG from 150 to 10 mg/L, and the removal of dye by $KRS_{0.5}$ increased from 41.58% to 86.86% with decreasing initial concentration of MG from 150 to 10 $mg \cdot L^{-1}$. Therefore, the adsorption percentage decreases and the extent of adsorption increases with increasing initial MG concentration. This is so because the initial dye concentration provides the driving force to overcome the resistance to the mass transfer of dye between the aqueous and the solid phase [25]. For constant dosage of the adsorbent, at higher initial dye concentration, the available adsorption sites

Table 2: Effect of initial concentration of MG on adsorption.

C_0 (mg/L)	$KRH_{0.5}$		$KRS_{0.5}$	
	q_e (mg/g)	%	q_e (mg/g)	%
10	24.93	92.28	23.37	86.86
20	54.81	91.42	50.49	84.15
25	69.21	91.35	64.91	77.92
50	137.2	86.62	112.9	73.17
80	206.9	87.32	147.2	62.12
100	262.0	83.24	156.7	53.27
125	302.9	80.37	179.1	47.67
150	324.2	74.64	180.1	41.58

of adsorbent become fewer, and hence the removal of MG depends upon the initial concentration.

3.3.2. Adsorption Isotherm. The adsorption isotherms express the specific relation between the concentration of adsorbate and its degree of accumulation onto adsorbent surface at a constant temperature [26]. Several isotherm models (Langmuir isotherm [27] and Freundlich isotherm [28]) have been used to fit to the experimental data and evaluate the isotherm performance for MG adsorption (Table 3).

(1) Langmuir Isotherm. It assumes that maximum adsorption corresponds to a saturated monolayer of solute molecules on the adsorbent surface, with each site carrying an equal number of adsorbed molecules and no interaction between adsorbate molecules [29, 30]. The expression of the Langmuir model is given by the following:

$$q_e = \frac{q_m K_L C_e}{1 + K_L C_e}, \quad (3)$$

where q_e (mg·g^{-1}) and C_e (mg·L^{-1}) are the amounts of MG adsorbed per unit mass of sorbent and MG concentration in solution at equilibrium, respectively, q_m (mg·g^{-1}) represents maximum monolayer adsorption capacity, and K_L (L·mg^{-1}) is the Langmuir adsorption constant related to binding energy for sorption.

The essential feature of the Langmuir model can be expressed in terms of a dimensionless constant separation factor (R_L) [27] given by the following equation:

$$R_L = \frac{1}{1 + K_L C_i}, \quad (4)$$

where k_L is the Langmuir constant (L/mg) and C_i is the initial MG concentration (mg/L). There are four probabilities for the R_L value: (i) for favorable adsorption, $0 < R_L < 1$, (ii) for unfavorable adsorption, $R_L > 1$, (iii) for linear adsorption, $R_L = 1$, and (iv) for irreversible adsorption, $R_L = 0$ [31].

The values of q_m and K_L calculated from the Langmuir model are tabulated in Table 2, and the calculated R_L values versus the initial MG concentrations are shown in Figure 4. The adsorption of $KRH_{0.5}$ and $KRS_{0.5}$ was more favorable at higher concentrations, and at low concentrations ($R_L = 0.972$, 0.896), it appears similar to linear isotherm case ($R_L = 1$). The R_L mean of all experimental data is in the range of 0-1 (0.972–0.670, 0.896–0.364), further confirming that the sample is favorable for the adsorption process of MG [25].

(2) Freundlich Isotherm. It assumes that the adsorption occurs on a heterogeneous surface at nonidentical sites with different energies of adsorption that are not always available [28]. The expression is as follows:

$$q_e = K_F C e^{1/n}, \quad (5)$$

Table 3: Adsorption isotherm parameters.

Samples	Langmuir isotherm			Freundlich isotherm		
	q_m (mg·g^{-1})	K_L (L·mg^{-1})	R^2	K_F (mg$^{1-(1/n)}$·L$^{1/n}$·g^{-1})	n	R^2
$KRH_{0.5}$	1119	0.00286	0.995	5.069	1.189	0.991
$KRS_{0.5}$	295	0.01165	0.993	9.821	1.673	0.972

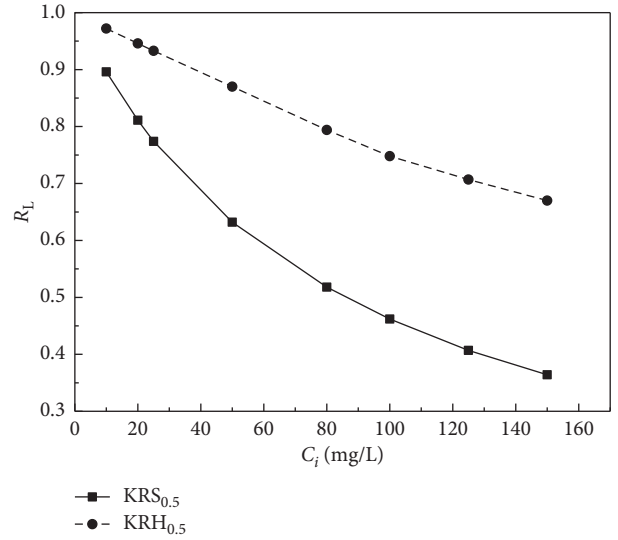

Figure 4: Plot of the separation factor for MG onto $KRH_{0.5}$ and $KRS_{0.5}$ versus the initial dye concentration.

where K_F is an indicator of the relative adsorption capacity of the adsorbent (mg$^{1-(1/n)}$·l$^{1/n}$/g) and n is that of the adsorption intensity, respectively.

The value of n, the Freundlich constant, was an empirical parameter that varied with the degree of heterogeneity and indicated the degree of nonlinearity between dye uptake capacity and unadsorbed dye in the solution and was related to the distribution of bonded ions on the sorbent surface [32]. In general, $n > 1$ suggested that the adsorbate was favorably adsorbed onto an adsorbent. As could be seen from the results of Table 2, the n values of the samples were all greater than 1.

The linear determined coefficients of the fitting lines of different isothermal equations are the tools used at most to indicate whether they are suitable for describing the adsorption reaction process. Fitting degree of $KRH_{0.5}$ was expressed as the Langmuir model > Freundlich model, while the fitting degree of $KRS_{0.5}$ was expressed as the Langmuir model > Freundlich model. According to the isothermal nonlinear adsorption curve in Figure 5, the theoretical equilibrium adsorption amount of each isothermal model corresponding to different initial concentration was fitted and was compared with the actual experimental data to indicate the conformity degree of different adsorption models to the adsorption system. The q_e calculated by the Langmuir equation was the closest to the experimental value. In conclusion, the best fit of equilibrium data in the Langmuir isotherm expression confirms the monolayer coverage of MG onto biochar particles.

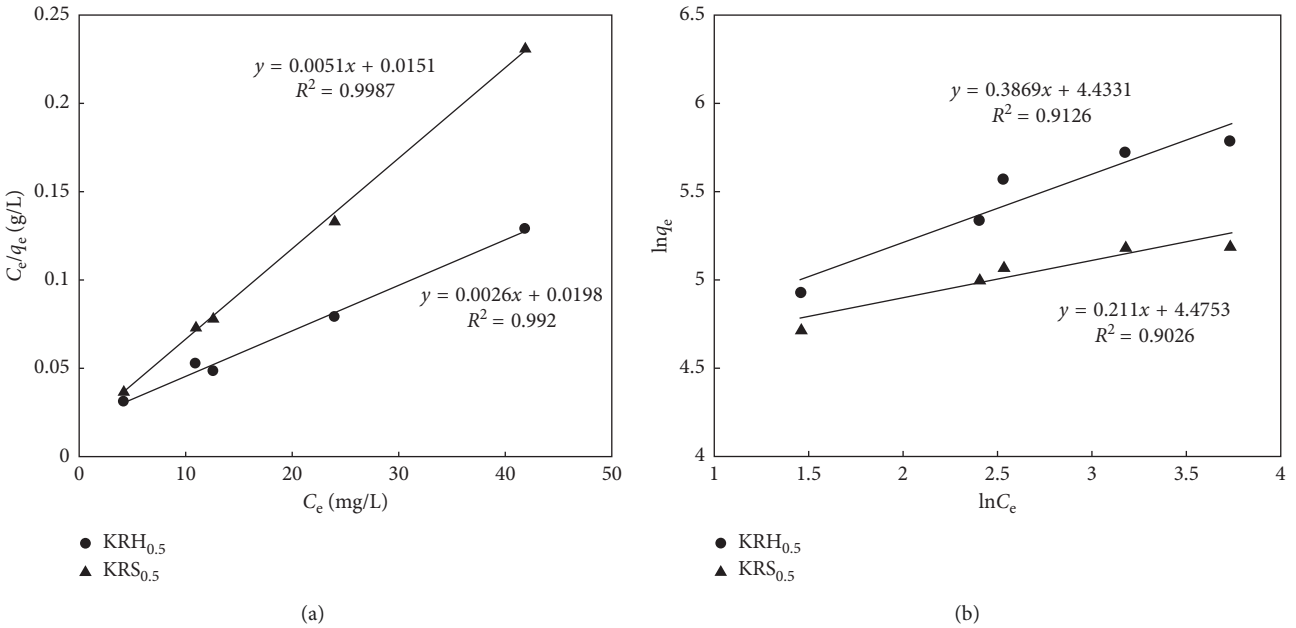

Figure 5: (a) Langmuir isotherms of $KRH_{0.5}$ on MG. (b) Freundlich isotherms of $KRS_{0.5}$ on MG.

3.4. Effect of Adsorption Time and Adsorption Kinetics

3.4.1. Pseudo-First-Order Kinetic Model. Assuming that the adsorption is controlled by the diffusion step, the single-layer adsorption completed through boundary diffusion is mainly described, which is expressed as follows [27]:

$$\frac{dq_t}{dt} = k_1(q_e - q_t). \tag{6}$$

After the boundary condition $t = 0$ to $t = t$ and $q_t = 0$ to $q_t = q_t$, the integral form of equation is

$$q_t = q_e\left(1 - e^{-k_1 t}\right). \tag{7}$$

3.4.2. Pseudo-Second-Order Kinetic Model. Assume that the adsorption is affected by the chemical adsorption rate, involving electron sharing or electron transfer between the adsorbent and the adsorbate. The whole adsorption process, including the complex adsorption reactions including external liquid film diffusion, surface adsorption, and intraparticle diffusion, can comprehensively reflect the adsorption kinetics mechanism between liquid and solid. The rate equation of the reaction can be expressed by the following expression [33]:

$$\frac{dq_t}{dt} = k_2\left(q_e - q_t\right)^2. \tag{8}$$

Integrating equation (8) for the boundary conditions $t = 0$ to $t = t$ and $q_t = 0$ to $q_t = q_t$ gives

$$q_t = \frac{q_e^2 k_2 t}{1 + q_e k_2 t}. \tag{9}$$

3.4.3. Elovich Equation. Assume that the active sites of the adsorbent are heterogeneous, showing different activation energies. During the adsorption process, as the surface coverage increases, the adsorption rate decreases with the increase of time, which is not suitable to describe the single reaction mechanism, which is generally expressed as follows [34]:

$$\frac{dq_t}{dt} = \alpha \exp\left(-\beta q_t\right). \tag{10}$$

Given that $q_t = 0$ at $t = 0$, the integrated form of equation (10) becomes

$$q_t = \frac{1}{\beta}\ln\left(t + t_0\right) - \frac{1}{\beta}\ln\left(t_0\right), \tag{11}$$

where $t_0 = 1/\alpha\beta$. If t is much larger than t_0, equation (11) can be simplified to

$$\begin{aligned} q_t &= \frac{1}{\beta}\ln(\alpha\beta) + \frac{1}{\beta}\ln(t), \\ q_t &= A + B\ln t. \end{aligned} \tag{12}$$

The nonlinear fitting results of the kinetic model are shown in Figures 6 and 7 and Table 4. The correlation coefficient R^2 of the pseudo-second-order kinetic equation was higher than that of the pseudo-first-order kinetic equation, and the theoretical adsorption capacity of the pseudo-second-order kinetic model was closer to the experimental measured value. The initial stage of adsorption can be described by both the pseudo-first-order kinetic and the pseudo-second-order kinetic models. In comparison, the pseudo-second-order kinetic model can well fit the whole adsorption process including the second half adsorption, external liquid film diffusion, surface adsorption, and internal diffusion of particles. From the correlation coefficient

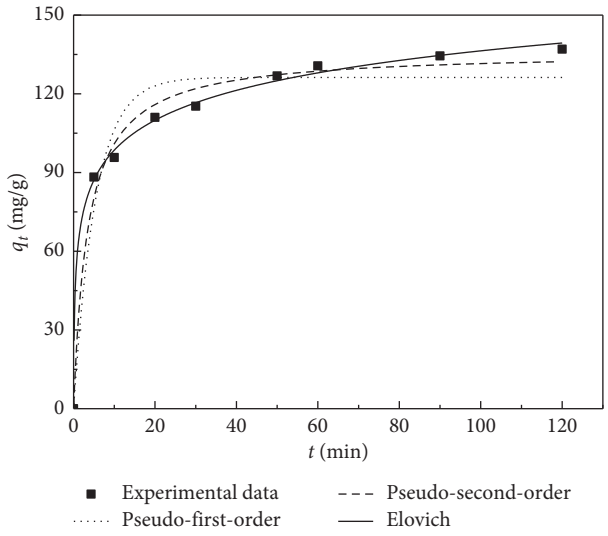

Figure 6: Adsorption kinetics of $KRH_{0.5}$ on MG.

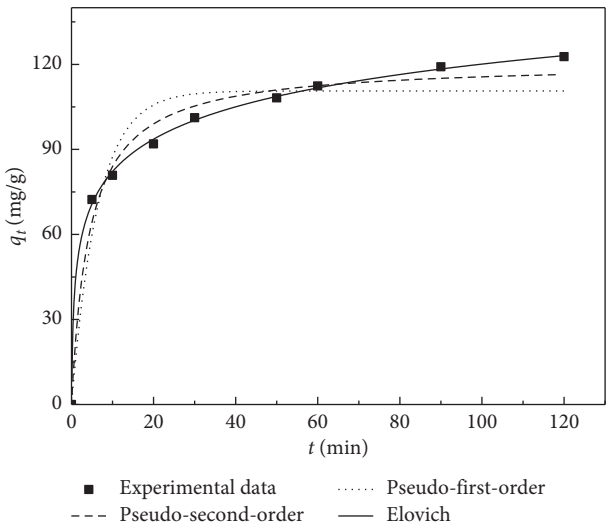

Figure 7: Adsorption kinetics of $KRS_{0.5}$ on MG.

R^2, it can be seen that the Elovich adsorption equation can well describe the adsorption process, indicating that the sample has uniformly distributed surface adsorption energy in the whole adsorption process.

3.5. Mechanism Study. The intraparticle diffusion process tends to control the adsorption rate in systems with high adsorption rates, high adsorption mass concentrations, and large adsorbent particle sizes. In order to understand the mechanism and rate control steps affecting the adsorption kinetics, the kinetic experimental results were fitted to Webber's intraparticle diffusion model and Boyd diffusion model [20].

3.5.1. Weber–Morris's Model. In the MG attachment process, the adsorption dynamics generally consist of three consecutive steps: (i) transport of adsorbate molecules from bulk solution to the outer surface of adsorbent (film diffusion); (ii) transport of the adsorbate molecules within the pores of the adsorbent, which occurs on the external surface (intraparticle diffusion or pore diffusion); (iii) sorption of the adsorbate molecules on the interior surfaces of the pores and capillary spaces of the adsorbent. To distinguish the dye adsorption process mechanism, the Weber–Morris equation is used for fitting the experimental data [23, 35]:

$$q_t = k_{id} t^{1/2} + C, \tag{13}$$

where q_t is the sorption capacity at time t ($mg \cdot g^{-1}$); C is the intercept; and k_{id} is the intraparticle diffusion rate constant ($mg \cdot g^{-1} \cdot min^{-1/2}$).

As shown in Figure 8, the process of $KRH_{0.5}$ and $KRS_{0.5}$ adsorbing MG was divided into three stages, which were consistent with the three steps of theoretical adsorption. In the first stage, the MG diffused to the surface of the sample through the liquid film, the resistance was small, the slope was the largest, and the adsorption rate was the fastest; in the second stage, the adsorption on the external surface had reached saturation, MG migrated from the adsorbent surface to the adsorption point, the adsorption on the inner surface increased, the diffusion resistance increased, and the adsorption rate gradually decreased; in the third stage, the saturation stage of MG adsorption, the adsorption tended to be balanced, which could be considered as instant completion. Fitting lines of the Weber–Morris's mode did not pass the origin, which indicated that the diffusion in particles was not the only limiting factor in the whole adsorption process, and there were other adsorption mechanisms.

3.5.2. Boyd Model. Assuming that the adsorption resistance is concentrated at the adsorbent particle boundary, the Boyd model can be used to identify the rate-limiting factors in the adsorption process, and its equation is as follows [23]:

$$F = \frac{q_t}{q_e} = 1 - \left[\frac{6}{\pi^2}\right] \sum_{n=1}^{\infty} \left(\frac{1}{n^2}\right) \exp\left(-n^2 B_t\right),$$

$$B_t = -0.4977 - \ln(1 - F), \quad F > 0.85, \tag{14}$$

$$B_t = \left(\sqrt{\pi} - \sqrt{\left(\pi - \frac{\pi^2 F}{3}\right)}\right)^2, \quad F < 0.85,$$

where F is the fractional attainment of equilibrium at different times t and B_t is a constant.

In the figure of B_t versus t (Figure 9), since the experiment used a higher concentration of MG and the mixing was more uniform, the fitted straight line did not pass through the origin, which indicated that the liquid film diffusion outside the particle was a limiting factor of the reaction rate and indicated intraparticle diffusion was also a limiting factor in the rate of reaction.

By measuring the isoelectric point, the pH_{pzc} values of RH and RS were 7.77 and 7.67, respectively, and the pH_{pzc} of KRH and KRS were 5.26 and 5.47, respectively. Under the

Table 4: Adsorption kinetic parameters.

	Pseudo-first-order kinetic model			Pseudo-second-order kinetic model			Elovich equation		
	q_1 (mg·g^{-1})	k_1 (min^{-1})	r_1^2	q_2 (mg·g^{-1})	k_2 (g·mg^{-1}·min^{-1})	r_2^2	A (mg·g^{-1})	B (g·mg^{-1}·min^{-1})	R_E^2
$KRH_{0.5}$	126.3	0.185	0.944	136.1	0.002	0.985	60.72	16.42	0.998
$KRS_{0.5}$	110.7	0.156	0.932	120.7	0.002	0.980	44.32	16.46	0.999

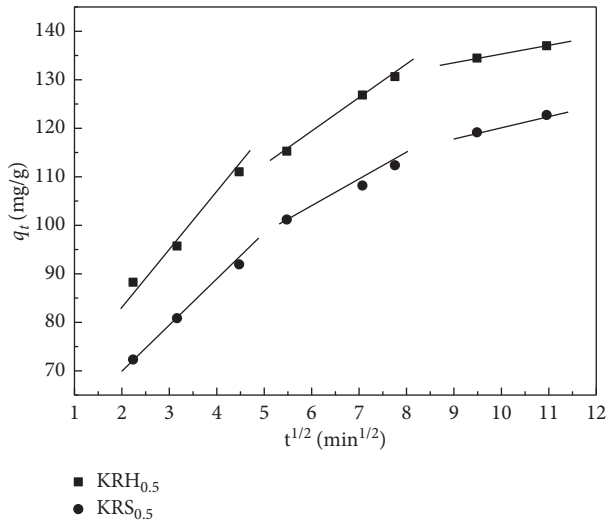

Figure 8: Intraparticle diffusion plots for the MG adsorption onto $KRH_{0.5}$ and $KRS_{0.5}$.

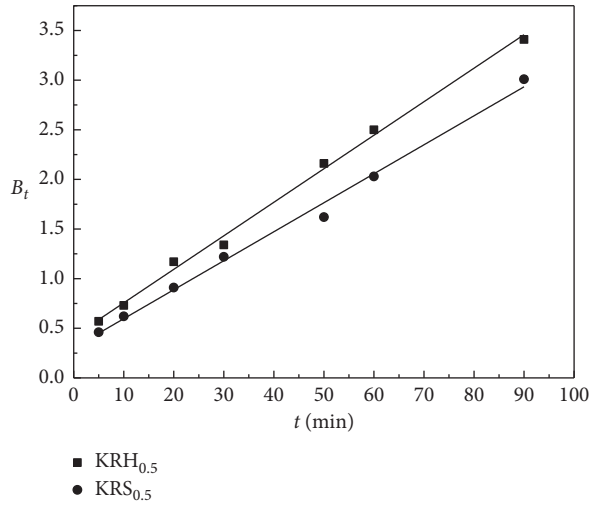

Figure 9: Boyd plot for adsorption of MG onto $KRH_{0.5}$ and $KRS_{0.5}$.

hydrothermal condition with $KMnO_4$ as the solute, the surface of biochar had a large number of acidic groups, mainly from acidic oxygen-containing functional groups such as carboxyl group and phenol hydroxyl group. They were acidic by dissociating protons, making the zero-electric point of biochar $pH_{pzc} < 7$. After the surface of biochar is modified by $KMnO_4$, the surface net charge of biochar and the nature of attractions between the molecules were suggested to be one of the reasons attributed for the adsorption capacity of biochar.

4. Conclusion

Rice husk (RH) and rice stalk (RS), the agricultural by-product waste, can be used as an effective alternative low-cost adsorbent for the removal of MG from wastewater. By the adsorption experiment results of MG, isoelectric point measurement, and FT-IR characterization, it was proved that there were a large number of acidic functional groups on the surface of $KRH_{0.5}$ and $KRS_{0.5}$. The adsorption reaction was affected by the initial dye concentration, adsorption time, dosage, etc. Considering the adsorption effect and economic benefits, 0.05 g samples were taken to adsorb 50 mg·L^{-1} at room temperature for 120 min, and the adsorption rate was verified for many times to be over 90%. The Langmuir isotherm model was the best for the description of the adsorption equilibrium of both dyes onto the biochar. The kinetic studies showed that the dye adsorption process followed Elovich kinetics models and the intraparticle diffusion was the control step of the adsorption rate, but it was not the only rate controlling step.

Data Availability

The data used to support the findings of this study are included within the article.

Conflicts of Interest

The authors declare that they have no conflicts of interest.

Acknowledgments

This work was supported by the Natural Science Foundation of Jilin Province Department of Education (nos. JJKH20170234KJ and JJKH20190857KJ).

References

[1] M. A. Ahmad, N. A. Ahmad Puad, and O. S. Bello, "Kinetic, equilibrium and thermodynamic studies of synthetic dye removal using pomegranate peel activated carbon prepared by microwave-induced KOH activation," *Water Resources and Industry*, vol. 6, pp. 18–35, 2014.

[2] G. Mckay and A. G. Sweeney, "Principles of dye removal from textile effluent," *Water, Air, and Soil Pollution*, vol. 14, no. 1, pp. 3–11, 1980.

[3] C. Ling, F.-Q. Liu, C. Long, T.-P. Chen, Q.-Y. Wu, and A.-M. Li, "Synergic removal and sequential recovery of acid black 1 and copper (II) with hyper-crosslinked resin and inside mechanisms," *Chemical Engineering Journal*, vol. 236, pp. 323–331, 2014.

[4] Y. Sun, Z. Chen, G. Wu et al., "Characteristics of water quality of municipal wastewater treatment plants in China:

implications for resources utilization and management," *Journal of Cleaner Production*, vol. 131, pp. 1–9, 2016.

[5] T. W. Seow and C. K. Lim, "Removal of dye by adsorption: a review," *International Journal of Applied Engineering Research*, vol. 11, no. 4, pp. 2675–2679, 2016.

[6] Y. Q. Ma, H. Yu, X. D. Li, Q. Z. Zhai, and J. B. Xu, "Adsorption of cadmium and chromium in water body by SBA-15," *Asian Journal of Chemistry*, vol. 22, no. 10, pp. 8219–8230, 2010.

[7] L. Li, J. Y. Liu, and Y. Wang, "Research on multi-index network DEA model," *Advanced Materials Research*, vol. 108–111, no. 3, pp. 1134–1140, 2010.

[8] J. J. Moreno-Barbosa, C. López-Velandia, A. D. P. Maldonado, L. Giraldo, and J. C. Moreno-Piraján, "Removal of lead(II) and zinc(II) ions from aqueous solutions by adsorption onto activated carbon synthesized from watermelon shell and walnut shell," *Adsorption*, vol. 19, no. 2–4, pp. 675–685, 2013.

[9] V. K. Gupta, A. Mittal, and V. Gajbe, "Adsorption and desorption studies of a water soluble dye, quinoline yellow, using waste materials," *Journal of Colloid and Interface Science*, vol. 284, no. 1, pp. 89–98, 2005.

[10] S. Uçar, M. Erdem, T. Tay, and S. Karagöz, "Removal of lead (II) and nickel (II) ions from aqueous solution using activated carbon prepared from rapeseed oil cake by Na_2CO_3 activation," *Clean Technologies and Environmental Policy*, vol. 17, no. 3, pp. 747–756, 2015.

[11] H. K. D. Nguyen, H. Q. Tran, N. L. T. Nguyen, and N. T. Dinh, "Study on the preparation of ordered mesoporous carbon-based catalyst from waste microalgal biomass for the synthesis of biokerosene," *Journal of Porous Materials*, vol. 25, no. 6, pp. 1567–1576, 2018.

[12] J. Bera and D. D. Kale, "Properties of polypropylene filled with chemically treated rice husk," *Journal of Applied Polymer Science*, vol. 110, no. 2, pp. 1271–1279, 2008.

[13] S. Rungrodnimitchai, "Modification of rice straw for heavy metal ion adsorbents by microwave heating," *Macromolecular Symposia*, vol. 295, no. 1, pp. 100–106, 2010.

[14] H. X. Zhang, X. F. Ding, X. Chen, Y. J. Ma, Z. C. Wang, and X. Zhao, "A new method of utilizing rice husk: consecutively preparing d-xylose, organosolv lignin, ethanol and amorphous superfine silica," *Journal of Hazardous Materials*, vol. 291, pp. 65–73, 2015.

[15] M. A. Islam, A. Benhouria, M. Asif, and B. H. Hameed, "Methylene blue adsorption on factory-rejected tea activated carbon prepared by conjunction of hydrothermal carbonization and sodium hydroxide activation processes," *Journal of the Taiwan Institute of Chemical Engineers*, vol. 52, pp. 57–64, 2015.

[16] S. Kang, X. Li, J. Fan, and J. Chang, "Characterization of hydrochars produced by hydrothermal carbonization of lignin, cellulose, d-xylose, and wood meal," *Industrial & Engineering Chemistry Research*, vol. 51, no. 26, pp. 9023–9031, 2012.

[17] A. Funke and F. Ziegler, "Hydrothermal carbonization of biomass: a summary and discussion of chemical mechanisms for process engineering," *Biofuels, Bioproducts and Biorefining*, vol. 4, no. 2, pp. 160–177, 2010.

[18] M.-M. Titirici, A. Thomas, and M. Antonietti, "Back in the black: hydrothermal carbonization of plant material as an efficient chemical process to treat the CO_2 problem?," *New Journal of Chemistry*, vol. 31, no. 6, pp. 787–789, 2007.

[19] S. Mustafa, B. Dilara, K. Nargis, A. Naeem, and P. Shahida, "Surface properties of the mixed oxides of iron and silica," *Colloids and Surfaces A: Physicochemical and Engineering Aspects*, vol. 205, no. 3, pp. 273–282, 2002.

[20] V. O. S. Neto, D. Q. Melo, T. C. de Oliveira et al., "Evaluation of new chemically modified coconut shell adsorbents with tannic acid for Cu(II) removal from wastewater," *Journal of Applied Polymer Science*, vol. 131, no. 18, pp. 40744–40755, 2014.

[21] Z. Z. Chowdhury, M. R. Hasan, S. B. A. Hamid, E. M. Samsudin, S. M. Zain, and K. Khalid, "Catalytic pretreatment of biochar residues derived from lignocellulosic feedstock for equilibrium studies of manganese, Mn(II) cations from aqueous solution," *RSC Advances*, vol. 5, no. 9, pp. 6345–6356, 2015.

[22] X. Cao and W. Harris, "Properties of dairy-manure-derived biochar pertinent to its potential use in remediation," *Bioresource Technology*, vol. 101, no. 14, pp. 5222–5228, 2010.

[23] L. Yu and Y. M. Luo, "The adsorption mechanism of anionic and cationic dyes by Jerusalem artichoke stalk-based mesoporous activated carbon," *Journal of Environmental Chemical Engineering*, vol. 2, no. 1, pp. 220–229, 2014.

[24] C. S. Ming, "Kinetics of the batch adsorption of methylene blue from aqueous solutions onto rice husk: effect of acid-modified process and dye concentration," *Desalination and Water Treatment*, vol. 37, no. 1–3, pp. 200–214, 2012.

[25] T. K. Sen, S. Afroze, and H. M. Ang, "Equilibrium, kinetics and mechanism of removal of methylene blue from aqueous solution by adsorption onto pine cone biomass of *Pinus radiata*," *Water, Air, & Soil Pollution*, vol. 218, no. 1–4, pp. 499–515, 2011.

[26] X. Liu and L. Zhang, "Removal of phosphate anions using the modified chitosan beads: adsorption kinetic, isotherm and mechanism studies," *Powder Technology*, vol. 277, pp. 112–119, 2015.

[27] I. Langmuir, "The constitution and fundamental properties of solids and liquids: part I—solids," *Journal of the American Chemical Society*, vol. 38, no. 11, pp. 2221–2295, 1916.

[28] H. M. F. Freundlich, "Over the adsorption in solution," *Journal of Physical Chemistry*, vol. 57, no. 385, pp. 4574–4578, 1906.

[29] R. Han, Y. Wang, P. Han, J. Shi, J. Yang, and Y. Lu, "Removal of methylene blue from aqueous solution by chaff in batch mode," *Journal of Hazardous Materials*, vol. 137, no. 1, pp. 550–557, 2006.

[30] D. D. Sewu, P. Boakye, and S. H. Woo, "Highly efficient adsorption of cationic dye by biochar produced with Korean cabbage waste," *Bioresource Technology*, vol. 224, pp. 206–213, 2017.

[31] M. T. Yagub, T. K. Sen, S. Afroze, and H. M. Ang, "Dye and its removal from aqueous solution by adsorption: a review," *Advances in Colloid and Interface Science*, vol. 209, no. 7, pp. 172–184, 2014.

[32] M. Sathishkumar, A. R. Binupriya, K. Vijayaraghavan, and S.-I. Yun, "Two and three-parameter isothermal modeling for liquid-phase sorption of procion blue H-B by inactive mycelial biomass of *Panus fulvus*," *Journal of Chemical Technology and Biotechnology*, vol. 82, no. 4, pp. 389–398, 2010.

[33] H. Ren, Z. Gao, D. Wu, J. Jiang, Y. Sun, and C. Luo, "Efficient Pb(II) removal using sodium alginate-carboxymethyl cellulose gel beads: preparation, characterization, and adsorption mechanism," *Carbohydrate Polymers*, vol. 137, pp. 402–409, 2016.

[34] P. H. Zhang, Y. C. Li, H. B. Hu, J. G. Zhao, and J. S. Wang, "Methylene blue adsorption characteristics onto biochar derived from Ginkgo biloba," *Environmental Pollution and Control*, vol. 39, no. 11, pp. 1229–1234, 2017.

[35] Y. Zhou, X. Liu, Y. Xiang et al., "Modification of biochar derived from sawdust and its application in removal of tetracycline and copper from aqueous solution: adsorption mechanism and modelling," *Bioresource Technology*, vol. 245, pp. 266–268, 2017.